DOI: 10.1002/cbic.200500285

Binding of Helix-Threading Peptides to *E. coli* 16S Ribosomal RNA and Inhibition of the S15–16S Complex

Barry D. Gooch, Malathy Krishnamurthy, Mohammad Shadid, and Peter A. Beal*[a]

Dedicated to Prof. Peter B. Dervan on the occasion of his 60th birthday

Helix-threading peptides (HTPs) constitute a new class of small molecules that bind selectively to duplex RNA structures adjacent to helix defects and project peptide functionality into the dissimilar duplex grooves. To further explore and develop the capabilities of the HTP design for binding RNA selectively, we identified helix 22 of the prokaryotic ribosomal RNA 16S as a target. This helix is a component of the binding site for the ribosomal protein S15. In addition, the S15–16S RNA interaction is important for the ordered assembly of the bacterial ribosome. Here we present the synthesis and characterization of helix-threading peptides that bind selectively to helix 22 of E. coli *16S RNA. These compounds bind helix 22 by threading intercalation placing the N termini in the minor groove and the C termini in the major groove. Binding is dependent on the presence of a highly conserved purine-rich internal loop in the RNA, whereas removal of the loop minimally affects binding of the classical intercalators ethidium bromide and methidiumpropyl–EDTA·Fe (MPE·Fe). Moreover, binding selectivity translates into selective inhibition of formation of the S15–16S complex.*

Introduction

Over the past two decades, increased awareness of RNA-dependent biological phenomena has spurred many attempts to develop RNA-binding small molecules.[1–3] While many designs have displayed varying levels of efficacy for particular targets, very few have achieved the selectivity necessary to discriminate effectively against non-target RNA molecules. This is particularly evident in the case of aminoglycosides.[4,5] Subsequent to the discovery of the prokaryotic ribosomal A-site binding pocket, many different naturally occurring and artificial RNA structures have been shown to support aminoglycoside binding. This promiscuity has prompted investigators to make various modifications to these compounds or turn to different chemical scaffolds in order to develop RNA-binding compounds with greater selectivity.[6,7]

Our laboratory has developed helix-threading peptides (HTPs) that target duplex RNA structures selectively by threading intercalation.[8–15] Early studies by Cech and Draper, as well as more recent efforts by us and others, have established that certain duplex-RNA structures are predisposed to high-affinity intercalation and can be selectively targeted by intercalating ligands.[12,13,15–21] Therefore, one approach to generating a highly selective RNA-binding compound is through modification of an intercalating ligand to maximize binding at one of these high-affinity sites, while minimizing nonselective binding to other double-helical structures. In duplex RNA, the major and minor grooves contain functional groups that provide unique recognition surfaces. The compounds we have developed have an intercalation domain substituted in such a way as to project peptide functional groups into these dissimilar grooves. Thus, affinity for the target RNA can be maximized through stabilizing interactions between the peptide and functional groups found in the grooves at that site. Furthermore, since HTPs bind by threading intercalation, a substantial opening of the duplex is required. Defects in RNA duplexes, such as bulges and loops, increase the rate of base-pair opening and may facilitate binding, while more conformationally rigid sites are refractory to these compounds.[22]

To further explore and develop the capabilities of the HTP design for binding RNA selectively, we identified helix 22 of the prokaryotic ribosomal 16S RNA as a target. This helix is a component of the binding site for the ribosomal protein S15 (Figure 1).[23,24] In addition, the S15–16S RNA interaction is important for the ordered assembly of the bacterial ribosome.[25–27] Here we present the synthesis and characterization of helix-threading peptides that bind selectively to helix 22 of *E. coli* 16S RNA. Binding of the threading intercalator is dependent on the presence of a highly conserved purine-rich internal loop in the RNA, whereas removal of the loop minimally affects binding of the classical intercalators ethidium bromide and

[a] *B. D. Gooch, M. Krishnamurthy, M. Shadid, Prof. P. A. Beal*
Department of Chemistry, University of Utah
315 South 1400 East, Salt Lake City, Utah 84112-0850 (USA)
Fax: (+1) 801-581-8433
E-mail: beal@chem.utah.edu

Supporting information for this article is available on the WWW under http://www.chembiochem.org or from the author.

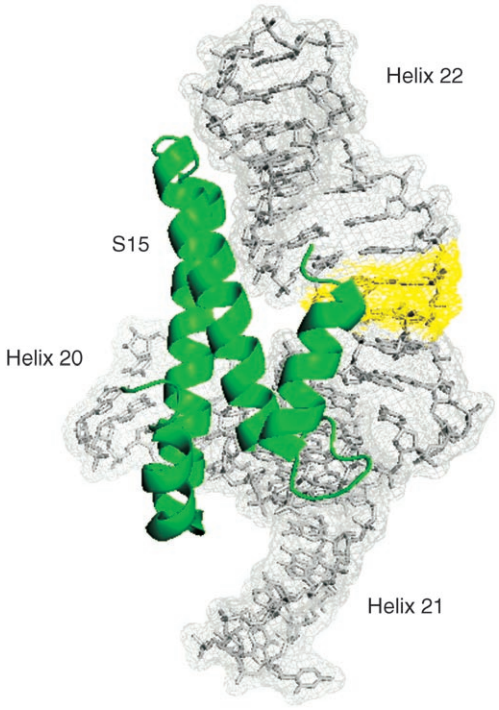

Figure 1. Structure of a ribonucleoprotein complex from the central domain of the *T. thermophilus* 30S ribosomal subunit depicting S15 bound to the junction of helices 20, 21, and 22.[24] The helix-threading peptide binding site is highlighted yellow.

methidiumpropyl-EDTA·Fe (MPE·Fe). Moreover, binding selectivity translates into selective inhibition of protein–RNA complex formation.

Results and Discussion

Recent in vitro selection experiments and structure–activity relationship studies have enabled us to define the minimal RNA structure that allows for optimum binding by helix-threading peptides.[12,13] Using these criteria, we identified a sequence within helix 22 of *E. coli* 16S RNA as a possible target. Interestingly, this notion was supported by the work of Kean et al. in which it was demonstrated that the classical intercalator ethidium bromide bound selectively to this site.[17] For our studies, a 61-nucleotide RNA construct was designed to mimic the 16S binding site for the S15 protein containing helix 22. Several HTPs were then synthesized in order to evaluate their ability to bind this RNA.

Synthesis of Fmoc-protected acridine amino acid

In order to accomplish the peptide synthesis, a new acridine-containing amino acid was prepared. We had previously reported a synthetic route to an acridine-containing amino acid protected as the allyloxycarbamate (Alloc).[8] However, the palladium-mediated removal of the Alloc group during peptide synthesis was time consuming due to the air- and moisture-sensitivity of this reaction. To circumvent these issues, a synthesis to the fluorenylmethoxycarbamate (Fmoc)-protected acridine amino acid was designed (Scheme 1). Commercially available 9-acridone-4-carboxylic acid was protected as the benzyl ester to give compound **1**, followed by chlorination at

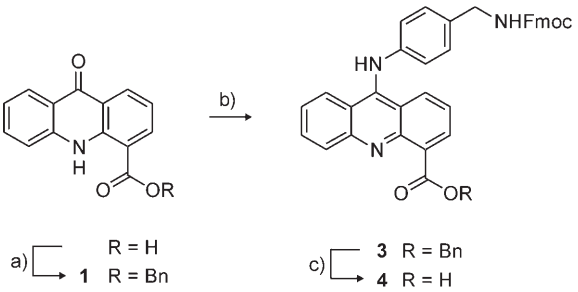

Scheme 1. Reagents and conditions: a) $BnBr/K_2CO_3$/DMF/RT, 88%; b) $POCL_3$/reflux/3 h, then (9-fluorenylmethyl)-4-aminobenzylaminocarbamate (**2**)/CH_3CN/reflux/10 min, 69%; c) H_2/10% Pd/C/MeOH/RT, 83%.

C9 and substitution with 9-fluorenylmethyl-4-aminobenzylaminocarbamate **2** to result in the fully protected amino acid **3**. Hydrogenolysis yielded the free carboxylic acid **4**, which was amenable to standard Fmoc solid-phase peptide synthesis protocols. The acridine-based amino acid was then incorporated into helix-threading peptide sequences (Scheme 2).

Helix-threading peptide binding site and orientation

The RNA-binding properties of several helix-threading peptides were evaluated, and HTP **5** (AcrDprLysLys; Acr refers to the acridine amino acid and Dpr is diamino propionic acid) was selected for further characterization (Scheme 2). To determine its binding site and orientation, **5** was modified with EDTA·Fe at either its N or C terminus to give the affinity cleaving reagents **6** and **7**, respectively. In the presence of reducing agents, EDTA·Fe generates diffusible hydroxyl radicals, which produce diagnostic cleavage patterns depending on whether the hydroxyl-radical generator is located in the minor or major groove of a double-helical nucleic acid structure.[28–32] After the 5′-^{32}P-labeled RNA construct had been treated with the affinity cleaving reagents, RNA fragments were separated under denaturing conditions by polyacrylamide gel electrophoresis (Figure 2A). The most efficiently cleaved nucleotides were mapped onto the RNA secondary structure (Figure 2B). Nucleotides cleaved by **6** (blue) and **7** (red) surround a 5′-CpG-3′ step that constitutes the proposed intercalation site. Although **7** cleaves the duplex with less selectivity than does **6**, this was not surprising given the previously observed behavior of C-terminal EDTA·Fe-modified compounds and RNA molecules of similar structure.[13] When transferred to the three-dimensional structure of this three-helix junction from *Thermus thermophilus* 16S RNA, the cleavage patterns clearly indicate that these compounds bind helix 22 by threading intercalation with the benzylamine substituent in the minor groove and the DprLysLys tripeptide in the major groove (Figure 2C).[24]

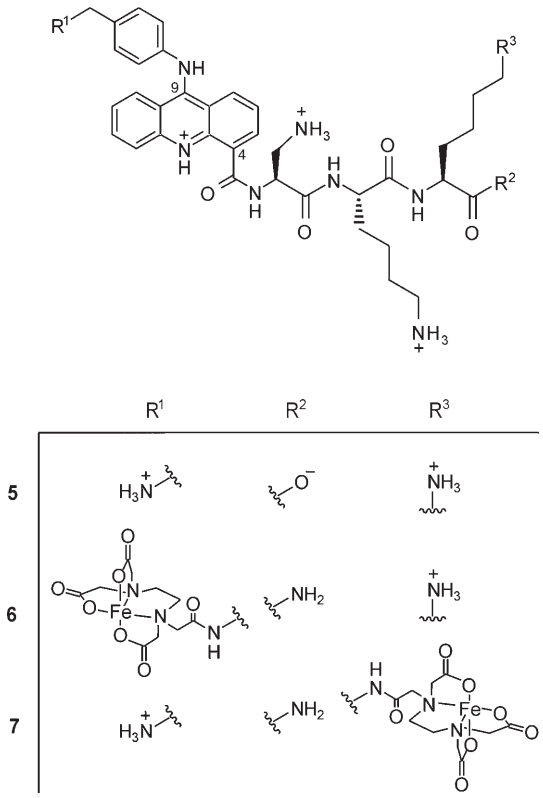

Scheme 2. Structures of helix-threading peptides **5**–**7**.

Contrasting binding selectivity of classical and threading intercalators

The putative intercalation site in helix 22 is the C660·G745–G661·C744 step, which is adjacent to the bulged A746 and near the highly conserved purine-rich internal loop consisting of A663, G664, A665, G741, and G742.[33] Our earlier studies with HTP-binding aptamers indicated that efficient binding by this type of ligand required helix defects on both sides of the intercalation site.[13] Therefore, we tested the effect of replacing the purine-rich loop of helix 22 with two C·G base pairs (A663C/G664Δ/A665C; Figure 3A). This change in RNA sequence had been shown by Ehresman to have no effect on S15-binding affinity.[33] However, this loop structure is thought to facilitate conformational changes that take place during the ribosomal-assembly process to allow for the binding of ribosomal proteins S6 and S18.[23] We also evaluated the effect that this change in RNA structure had on the binding of ethidium bromide and MPE·Fe, since these compounds were also known to bind this site in helix 22.[17,21]

At a concentration of 5 μM, both HTP **6** and MPE·Fe result in similar cleavage patterns on the wild-type *E. coli* construct (Figure 3B). However, the mutant RNA, which lacks the internal loop, does not support selective binding by the HTP, as indicated by the inefficient cleavage of this RNA by **6** (Figure 3B). Considering the MPE·Fe-cleavage efficiency on the mutant RNA, removal of the internal loop appeared to have a minimal effect on its binding. The contrasting dependencies on the internal loop exhibited by the two intercalators suggest that RNA structure determinants for efficient binding by a helix-

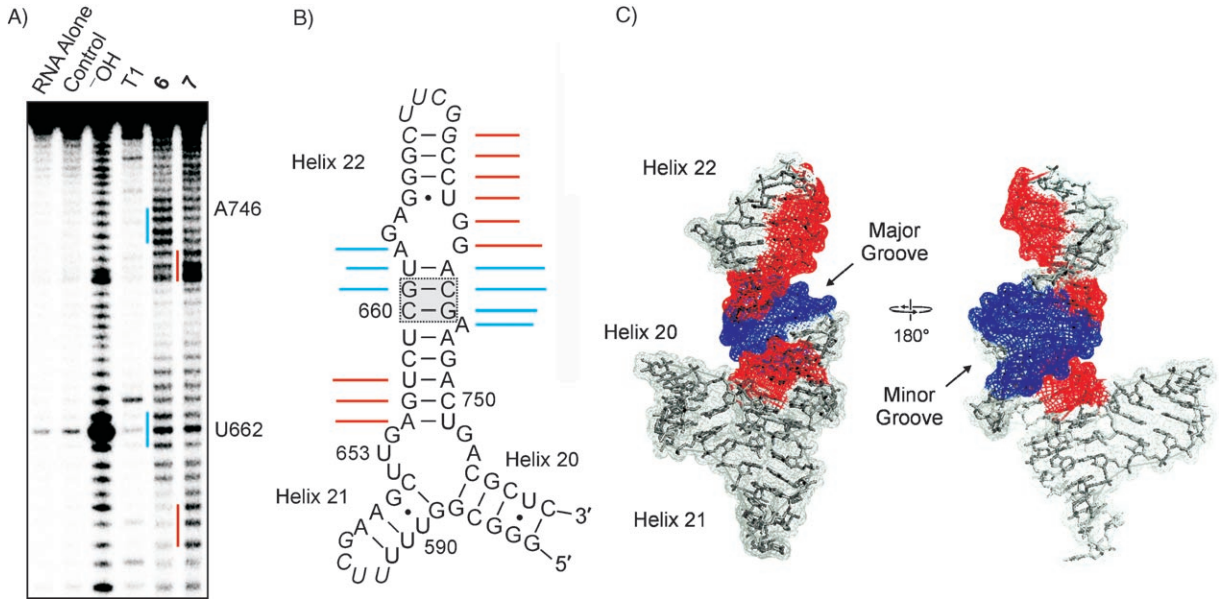

Figure 2. A) 5′-^{32}P-labeled affinity cleavage products of the wild-type RNA construct. Lanes from left to right: RNA alone; EDTA (25 μM), $Fe(NH_4)_2(SO_4)_2$ (50 μM), and **5** (25 μM); alkaline hydrolysis; RNase T1 reactivity at guanosine; **6** (7 μM); **7** (25 μM). Bracketed regions show the nucleotides most efficiently cleaved by **6** (blue) and **7** (red). Upper (3′) region cleaved by **7** contains nucleotides that could not be individually resolved, but comprises G737–G741. B) Predicted secondary structure of the RNA construct showing location and efficiency of hydroxyl radical cleavage by **6** (blue) and **7** (red). The putative intercalation site is highlighted gray. Nucleotides G737–G741 could not be individually resolved and are displayed with equal cleavage efficiencies. Italicized nucleotides are not native sequence, but incorporated to facilitate formation of the RNA structure. C) Two orientations of the structure of a three-helix junction from the central domain of the *T. thermophilus* 30S ribosomal subunit depicting the location of nucleotides cleaved by **6** (blue) and **7** (red).[24]

threading peptide are more stringent than those for classical intercalation and result in the selectivity observed in the affinity cleaving experiments.

Quantitative binding experiments were carried out to complement the qualitative studies with the EDTA·Fe-modified compounds described above. Ribonuclease V1 footprinting of the wild-type and mutant RNA constructs with **5** and ethidium bromide confirm the affinity cleaving results (Figure 4). Ethidium bromide binds well to both wild-type and mutant RNA constructs with only a fourfold difference in measured dissociation constants (Table 1). However, HTP **5** binds to wild-type helix 22 with at least a 30-fold preference, since no protection from the nuclease could be observed even at the highest concentration tested (500 μM).

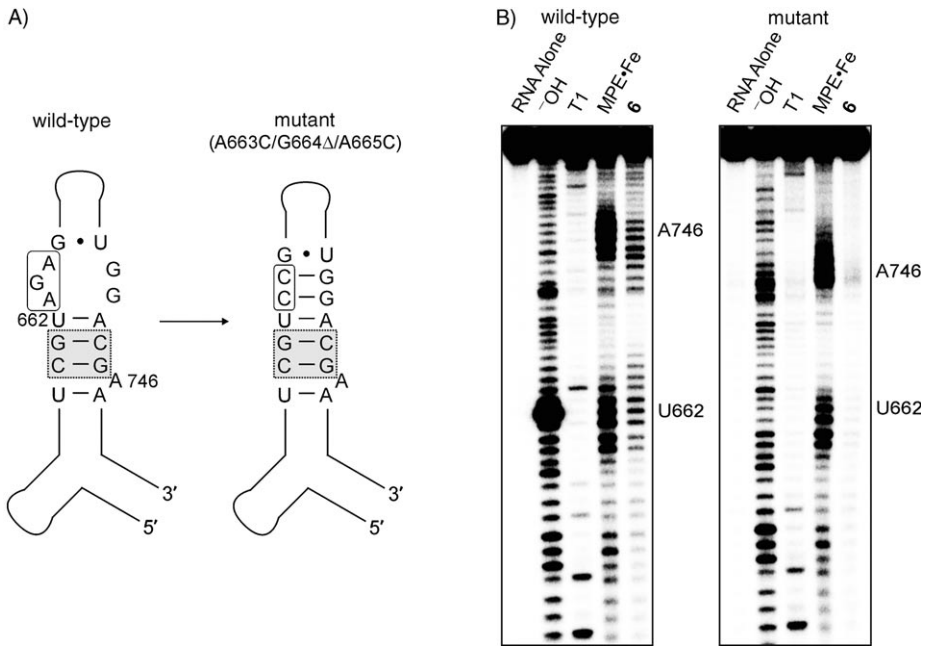

Figure 3. A) RNA sequence and predicted secondary structure near the helix-threading peptide binding site of helix 22 in the wild-type and mutant RNA constructs. The putative intercalation site is highlighted gray. B) 5′-^{32}P-labeled affinity cleavage products of the wild-type and mutant RNA constructs. Lanes from left to right (for both): RNA alone; alkaline hydrolysis; RNase T1 reactivity at guanosine; MPE·Fe (5 μM); **6** (5 μM).

Requirement for conformational flexibility in the RNA target

While carrying out these experiments, we noted that U662 in the wild-type helix 22 sequence is hyperreactive during alkaline hydrolysis (Figure 3B). This type of hydrolytic hyperreactivity is often seen in flexible sites in folded RNAs, such as in loops or bulges.[34] U662 is predicted to be base paired in the structure and adjacent to the A663·G742 pair of the purine-rich loop. When the loop sequence is mutated to create two C·G base pairs (A663C/G664Δ/A665C), alkaline hydrolysis hyperreactivity at U662 is lost, along with HTP binding (Figure 3B). This correlation is consistent with a link between conformational flexibility at the binding site and efficacy of HTP binding. It is interesting to note that conformational flexibility in 16S RNA at this site is a functional requirement that facilitates the ordered binding of ribosomal proteins.[23] It also appa-

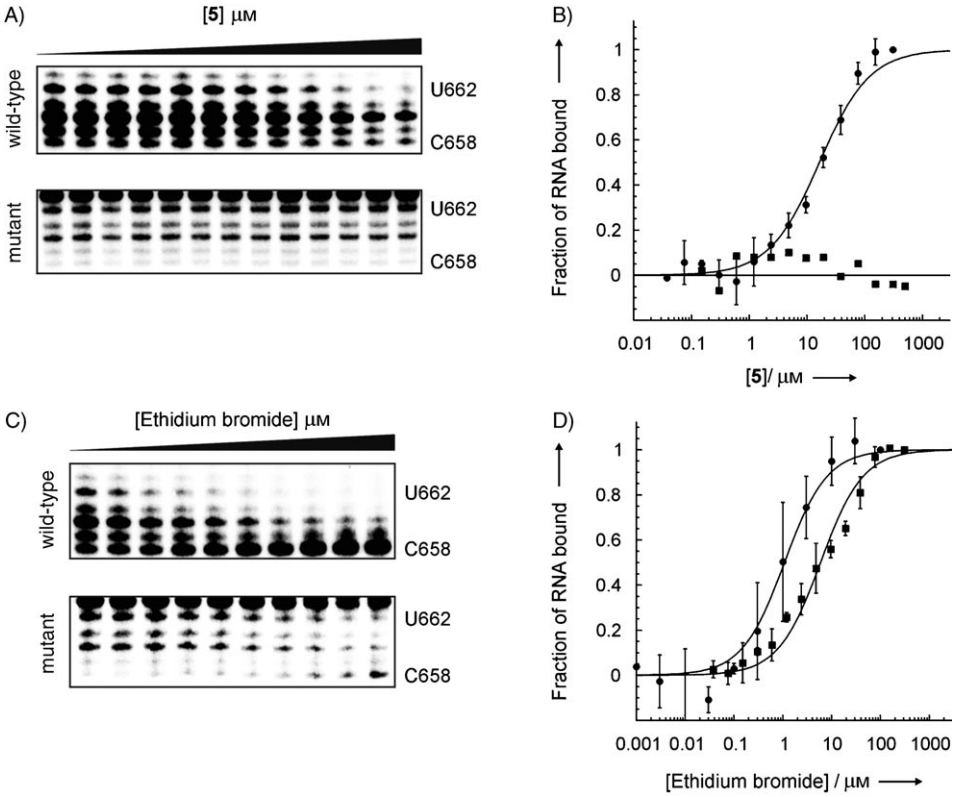

Figure 4. A) 5′-^{32}P-labeled RNase V1 cleavage products of the wild-type and mutant RNAs with increasing [**5**] (twofold increments from 0.15 to 307.2 μM). B) Plot of binding isotherms for **5** on wild-type (●) and mutant (■) RNA constructs. C) 5′-^{32}P-labeled RNase V1 cleavage products of the wild-type and mutant RNAs with increasing [ethidium bromide] (twofold increments from 0.15 to 76.8 μM). D) Plot of binding isotherms for ethidium bromide on wild-type (●) and mutant (■) RNA constructs.

Table 1. Dissociation constants of HTP **5** and ethidium bromide for the wild-type and mutant RNA constructs measured by quantitative ribonuclease V1 footprinting.

Compound	K_d (wild-type) [μM]	K_d (mutant) [μM]
AcrDprLysLys (**5**)	16.7 ± 3.1	>500
ethidium bromide	1.0 ± 0.8	4.3 ± 3.2

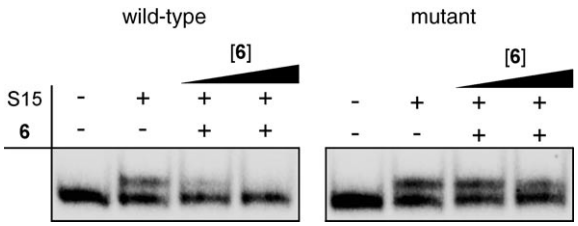

Figure 5. Gel mobility shift assay showing resolution of free wild-type and mutant RNA constructs from their respective complexes with S15 in the absence and presence of HTP **6** (5 and 10 μM).

rently allows for selective binding by helix-threading peptides. The identification of other RNAs with flexible duplex structures, in which the flexibility is a conserved feature of the RNA because of its functional importance, will likely reveal additional targets for control by HTPs.

Helix-threading peptide mediated inhibition of a protein–RNA complex

The HTP binding site in helix 22 of 16S RNA overlaps that of ribosomal protein S15 (Figure 1). S15 binds to the three-helix junction formed by the intersection of helices 20, 21, and 22. Interestingly, the observation that ethidium bromide binds selectively to this site in 16S RNA was made before the structure of the S15–16S complex was known.[21,24] The structure of the protein–RNA complex suggested to us that binding of an intercalating ligand into the helix 22 site might inhibit S15 binding. In addition, if this could be carried out with HTPs, affinity and selectivity optimization would be possible, since these compounds are constructed in a rapid, modular, solid-phase synthesis. Importantly, S15 is a primary binding protein in the ordered assembly of the bacterial 30S subunit.[25] Therefore, the S15–16S complex has been identified as a potential target for the development of new antibacterial agents that block growth by inhibiting ribosome assembly.[35]

To evaluate the effect HTP binding has on S15–16S association, we developed a gel mobility shift assay that allows for the resolution of free three-helix junction RNA from the S15–RNA complex. We chose to test the effect HTP **6** has on this interaction, since we had observed that **6** bound the target with higher affinity than **5**. This is most likely due to the fact that **5** places its negatively charged C-terminal carboxylate in the major groove, whereas **6** has a neutral C-terminal carboxamide. Importantly, **6** inhibits the binding of S15 to the three-helix junction RNA (Figure 5). To the best of our knowledge, this is the first successful attempt at inhibiting this interaction with a small molecule. Furthermore, the inhibition is selective for the wild-type sequence, as expected if HTP binding to helix 22 is the cause. Nearly complete inhibition of S15 binding to the wild-type sequence is observed at 5 μM HTP **6**, whereas this concentration has little effect on the complex with the mutant sequence (Figure 5). This difference is not due to a change in protein–RNA affinity, as the two RNAs bind S15 with nearly identical dissociation constants (wild-type: $K_d = 57 \pm 32$ nM, mutant: $K_d = 68 \pm 16$ nM, see Supporting Information). We have noted that the selectivity of the inhibition by **6** observed in the gel mobility shift assay is not absolute, since concentrations of **6** greater than 50 μM block binding to the mutant sequence as well. At these higher concentrations, nonselective, inefficient cleavage is observed with **6** and the mutant RNA. We suggest this nonselective binding is a result of the number of primary amines in this peptide and the resulting overall positive charge of the ligand. Future optimization will involve modifications that reduce the overall charge while improving target-site affinity.

Conclusion

We have shown that helix-threading peptides can bind selectively to helix 22 of *E. coli* 16S RNA. Complexation is highly dependent on the presence of a purine-rich internal loop. The classical intercalators ethidium bromide and MPE·Fe bind less selectively, since their affinity for the RNA is less dependent on the presence of the native loop structure. Binding of an HTP to this site in 16S RNA inhibits the association with the ribosomal protein S15. These studies extend our understanding of the structural requirements in naturally occurring RNAs for binding by HTPs. Since these compounds are prepared by using a modular, solid-phase synthesis, affinity and selectivity optimization is readily envisaged by the introduction of additional recognition elements into the groove-localized domains. Furthermore, because S15 is a primary binding protein in the ordered assembly of the bacterial ribosome, compounds that block the S15–16S interaction could be developed into antibacterial agents that inhibit growth by preventing ribosome assembly.

Experimental Section

General. All reagents for the synthesis of 9-(4′-methylamino-9-flourenylmethyloxycarbamate) anilinoacridine-4-carboxylic acid (**6**) were obtained from commercial sources and were used without further purification unless noted otherwise. Glassware for all reactions was oven dried at 125 °C overnight and cooled in a dessicator prior to use. All reactions were carried out under an argon atmosphere. Liquid reagents were introduced by oven-dried glass syringes. Tetrahydrofuran was distilled over sodium metal and benzophenone under an argon atmosphere, while acetonitrile was distilled over CaH_2. To monitor the progress of reactions, thin layer chromatography was performed with Merck silica gel 60 F254-precoated plates and alumina plates, eluting with the solvents indicated. Yields were calculated for material that appeared as a single spot by TLC and homogeneous by ^{1}H NMR. Short- and long-wavelength visualizations were performed with a Mineral light multiband ultraviolet lamp at 254 and 365 nm, respectively. Flash column chroma-

tography was carried out by using Mallinckrodt Baker silica gel 150 (60–200 mesh) and Fisher Alumina Adsorption gel (A540, 80–200 mesh). ^{1}H and ^{13}C NMR spectra of pure compounds were acquired on VXL-300, VXR-500 or Inova-500 spectrometers at 300, 500, 75, and 125 MHz. Chemical shifts for proton and carbon NMR are reported in parts per million with reference to the solvent peak. High-resolution chemical ionization (CI) and fast atom bombardment (FAB) spectra were recorded on a Finnigan MAT 95 mass spectrometer.

All reagents for solid-phase peptide synthesis (SPPS) were purchased from NovaBiochem (San Diego, CA), except for Fmoc-Dpr-(Boc)-OH (Advanced ChemTech, Louisville, KY), ethylenediaminetetraacetic acid (EDTA) monoanhydride, which was synthesized according to reported procedures,[36] and where otherwise noted. Ethidium bromide (1%) was obtained from Fisher Biotech (Fairlawn, NJ). Reagents for DNA amplification, RNA synthesis/radioactive labeling, hydroxyl-radical cleavage, and ribonuclease footprinting were purchased from Amersham Pharmacia Biotech: high-purity solution NTP set (ATP/CTP/GTP/UTP, 100 mM), RNase-Free deoxyribonuclease I (DNase I), RNAguard ribonuclease inhibitor (porcine); New England Biolabs: T4 polynucleotide kinase (PNK); Perkin–Elmer Life Sciences: [γ-^{32}P]ATP (6000 Ci mmol^{-1}); Stratagene: Pfu Turbo DNA polymerase; USB: PCR nucleotide mix (dATP/dCTP/dGTP/dTTP, 10 mM) and shrimp alkaline phosphatase (SAP). All commercial reagents were used as purchased without further purification. Chemically synthesized ribonucleic acids were purchased from the DNA/Peptide Core Facility at the University of Utah Health Sciences Center (HSC). Electrospray ionization (ESI) mass spectra were recorded on a Finnigan LCQ ion-trap mass spectrometer. Storage phosphor autoradiography was carried out and analyzed by using Molecular Dynamics imaging screens, Typhoon 9400 phosphorimager and ImageQuant 5.2 software.

Benzyl-9(10*H*)-acridone-4-carboxylate (1). Benzyl bromide (0.214 mL, 1.804 mmol) was added dropwise to a solution of 9-(10*H*)-acridone-4-carboxylic acid (0.216 g, 0.902 mmol) and K_2CO_3 (0.374 g, 2.706 mmol) in dry DMF (5 mL). The resulting solution was stirred at ambient temperature for 12 h under argon. TLC (50% EtOAc/hexanes) indicated complete conversion. The DMF was removed by adding water, and the product was extracted in EtOAc. The EtOAc layer was dried over anhydrous Na_2SO_4, and the solvent was removed under reduced pressure. Purification by silica gel column chromatography (15% EtOAc/hexanes) afforded 0.262 g (88%) of the product as a bright yellow solid. ^{1}H NMR (300 MHz, $CDCl_3$) $\delta = 8.70$ (d, $J = 7.8$ Hz, 1H), 8.43 (d, $J = 7.6$ Hz, 2H), 7.66 (t, $J = 7.7$ Hz, 1H), 7.52–7.19 (m, 8H), 5.44 (s, 2H); ^{13}C NMR (75 MHz, $CDCl_3$) $\delta = 177.91$, 167.84, 141.89, 140.12, 136.75, 135.47, 134.16, 134.07, 128.95, 128.81, 128.45, 127.16, 122.51, 121.62, 119.99, 117.69, 113.62, 67.38; high-resolution CI-MS calcd for $C_{21}H_{15}NO_3$: *m/z* 329.1052, found: 330.1125 $[M+H]^+$.

(9-Fluorenylmethyl)-4-aminobenzylaminocarbamate (2). Fmoc-OSu (1.0 g, 2.96 mmol) was added to a solution of 4-aminobenzylamine (0.434 g, 3.56 mmol) in freshly distilled THF (8 mL) and dichloromethane (2 mL). The resulting solution was treated with Et_3N (450 μL) and stirred at ambient temperature under argon for 2 h. TLC (5% MeOH/$CHCl_3$) indicated formation of the product. The solvent was removed under reduced pressure. Purification by silica gel column chromatography (2% MeOH/CH_2Cl_2) afforded 0.620 g (60%) of the product as a white solid. ^{1}H NMR (300 MHz, $CDCl_3$) $\delta = 7.76$ (d, $J = 7.3$ Hz, 2H), 7.59 (d, $J = 7.3$ Hz, 2H), 7.40 (t, $J = 7.3$ Hz, 2H), 7.31 (t, $J = 7.3$ Hz, 2H), 7.06 (d, $J = 8.1$ Hz, 2H), 6.63 (d, $J = 8.3$ Hz, 2H), 5.03 (s, 1H), 4.43 (d, $J = 6.8$ Hz, 2H), 4.26–4.19 (m, 3H), 3.60 ppm (br s, 2H); ^{13}C NMR (75 MHz, $CDCl_3$) $\delta = 156.52$, 146.04, 144.15, 141.49, 129.13, 128.37, 127.83, 127.22, 125.33, 120.15, 115.37, 66.75, 47.45, 44.93; high-resolution CI-MS calcd for $C_{22}H_{20}N_2O_2$: *m/z* 344.1525, found 345.1597 $[M+H]^+$.

Benzyl-9-(4′-methylaminofluorenylmethyloxycarbamate) anilinoacridine-4-carboxylate (3). A solution of **1** (0.051 g, 0.154 mmol) in $POCl_3$ (1.5 mL) was heated at reflux for 3 h. The reaction mixture was then cooled in ice and quenched by adding cold water. The resulting solution was neutralized by adding $NaHCO_3$ until the pH was alkaline. The product was then extracted with dichloromethane. The organic layer was dried over anhydrous Na_2SO_4, and the solvent was removed under reduced pressure to obtain the benzyl-9-chloroacridine-4-carboxylate intermediate. The residue was then dissolved in freshly distilled acetonitrile (5 mL). (9-Fluorenylmethyl)-4-aminobenzylaminocarbamate (**2**; 0.079 g, 0.231 mmol) was added to this solution, and the reaction mixture was heated at reflux for 10 min. TLC (5% MeOH/$CHCl_3$) indicated complete disappearance of the chloro intermediate. The solvent was removed under reduced pressure. The residue was then dissolved in CH_2Cl_2 and extracted with brine. The organic layer was dried over anhydrous Na_2SO_4, and the solvent was removed under reduced pressure. Purification by alumina gel column chromatography (10% EtOAc/hexanes) afforded 0.070 g (69%, over two steps) of the product as a bright orange solid. ^{1}H NMR (500 MHz, $CDCl_3$) $\delta = 11.16$ (br s, 1H), 8.71 (br s, 1H), 8.23 (s, 1H), 7.74 (d, $J = 7.3$ Hz, 2H), 7.59 (d, $J = 6.8$ Hz, 2H), 7.47–7.34 (m, 7H), 7.29 (t, $J = 7.3$ Hz, 2H), 7.20 (d, $J = 7.3$ Hz, 2H), 7.15 (d, $J = 8.3$ Hz, 1H), 6.79 (d, $J = 6.8$ Hz, 2H), 5.42 (s, 2H), 5.05 (s, 1H), 4.46 (d, $J = 6.8$ Hz, 2H), 4.37 (d, $J = 4.4$ Hz, 2H), 4.23 (t, $J = 6.4$ Hz, 1H); ^{13}C NMR (125 MHz, $CDCl_3$) $\delta = 168.16$, 156.65, 152.91, 151.36, 144.19, 141.56, 135.76, 134.41, 131.75, 129.29, 128.97, 128.94, 128.75, 128.40, 127.89, 127.27, 125.22, 121.21, 120.18, 119.95, 118.73, 117.73, 107.96, 67.19, 66.85, 47.58, 45.15; high-resolution FAB-MS calcd for $C_{43}H_{33}N_3O_4$: *m/z* 655.2471, found 656.2515 $[M+H]^+$.

9-(4′-Methylamino-9-fluorenylmethyloxycarbamate) anilinoacridine-4-carboxylic acid (4). A suspension of **3** (0.070 g, 0.107 mmol) and 10% palladium on carbon (5 mg) in methanol (5 mL) was opened to vacuum and refilled three times with hydrogen gas through a balloon. The reaction mixture was stirred for 12 h at ambient temperature, at which point TLC (15% MeOH/$CHCl_3$) indicated completion of the reaction. The solution was filtered through a Celite pad, and the filtrate was concentrated under reduced pressure. Purification by silica gel column chromatography (3–4% MeOH/$CHCl_3$) afforded 0.050 g (83%) of the product as a bright orange solid. ^{1}H NMR (500 MHz, [D$_6$]DMSO) $\delta = 8.48$ (br s, 1H), 8.37 (br s, 1H), 7.87 (d, $J = 7.3$ Hz, 2H), 7.83 (t, $J = 6.1$ Hz, 2H), 7.69 (d, $J = 7.8$ Hz, 2H), 7.52–7.51 (m, 1H), 7.38 (t, $J = 7.6$ Hz, 3H), 7.30 (t, $J = 7.3$ Hz, 3H), 7.18 (d, $J = 8.3$ Hz, 2H), 6.99 (br s, 2H), 4.36 (d, $J = 6.8$ Hz, 2H), 4.22 (t, $J = 6.8$ Hz, 1H), 4.18 (d, $J = 5.9$ Hz, 2H), 4.09 (br s, 1H); ^{13}C NMR (125 MHz, [D$_6$]DMSO) $\delta = 167.81$, 156.36, 156.31, 150.41, 143.87, 140.75, 135.62, 132.79, 130.44, 128.27, 127.82, 127.62, 127.51, 127.01, 126.98 125.19, 125.07, 123.41, 121.85, 120.14, 120.03, 119.14, 119.04, 117.17, 65.26, 46.79, 43.35; high-resolution FAB-MS calcd for $C_{36}H_{27}N_3O_4$: *m/z* 565.2002, found: 566.2056 $[M+H]^+$.

NH_2-AcrDprLysLys-CO_2H (5). TentaGel OH Macrobead resin from Rapp Polymere GmbH (Tübingen, Germany, 0.21 mmol g^{-1}, 50 mg, 0.011 mmol) was added to a BioRad Poly-Prep column and swollen in DMF. A solution of Fmoc-Lys(Boc)-OH (5 equiv), *N*-hydroxybenzotriazole (HOBt; 5 equiv), and 2-(1*H*-benzotriazole-1-yl)-1,1,3,3-tetramethyluronium hexafluorophosphate (HBTU; 5 equiv) in DMF was added to the resin, followed immediately by addition of diisopropylethylamine (DIPEA; 10 equiv). The resin was agitated for approx-

imately 5 h at ambient temperature, then washed consecutively with DMF and MeOH. After swelling in DMF, the resin was treated with 20% piperidine in DMF (3×3 min) to remove the *N*-terminal Fmoc protecting group, then washed. The subsequent amino acids, Fmoc-Lys(Boc)-OH, Fmoc-Dpr(Boc)-OH, and Fmoc-Acr-OH (**4**) were coupled in an identical manner. Following Fmoc deprotection of the acridine residue, the resin was washed and dried by aspirating and lyophilizing overnight. The dry resin was treated with trifluoroacetic acid (TFA)/PhOH/H_2O/triisopropylsilane (TIPS; 88:5:5:2) for 1 h at ambient temperature to remove remaining acid-labile protecting groups. After consecutive washes with CH_2Cl_2, DMF, and MeOH, the resin was aspirated to dryness and lyophilized for approximately 5 h. The dry resin (~5 mg) was placed in one well of a MultiScreen® Solvinert 96-well filter plate (Millipore) and agitated with NaOH (170 μL, 0.1 N) for 1 h at ambient temperature. This slurry was neutralized with HCl (2 N) and buffered with Bis-Tris (50 mM, pH 7), and agitated for an additional 1 h. An ~2 mM solution of the released product was collected by vacuum filtration. The product was purified by HPLC on a reversed-phase C-18 column (4.6×250 mm, Vydac) following absorbance of the compound at λ_{max} = 442 nm. The compound was eluted with a gradient of H_2O (0.1% TFA; mobile phase A) and 60% acetonitrile (ACN; 0.1% TFA; mobile phase B; 0–4 min, linear increase to 40% B; 4–16 min, linear increase to 80% B; 16–17 min, linear increase to 100% B; 1 mL min^{-1}). HTP **5** was analyzed by ESI-MS, calcd molecular weight: 685.4; found: 686.3 $[M+H]^+$.

EDTA·Fe-AcrDprLysLys-CONH$_2$ (6). Rink amide 4-methylbenzhydrylamine (MBHA) resin (0.64 mmol g^{-1}, 25 mg, 0.016 mmol) was added to a Bio-Rad Poly-Prep column and swollen in DMF; this was followed by deprotection of the Fmoc group with 20% piperidine in DMF (3×3 min). The Fmoc-protected amino acid couplings of apo-**6** were identical to the preparation of **5**. Following Fmoc deprotection of the acridine residue, the resin was washed and dried by aspirating and lyophilizing for approximately 3 h. EDTA-monoanhydride (10 equiv), dissolved in warm anhydrous DMF, was added to the resin, and the reactor was agitated for 17 h at ambient temperature. The resin was washed and dried/lyophilized, then treated with TFA/PhOH/H_2O/TIPS (88:5:5:2) for 3 h at ambient temperature to remove remaining protecting groups and to release the tethered compound. The solution containing apo-**6** was collected and concentrated under reduced pressure. Diethyl ether precipitation of the residue, followed by extraction with water and neutralization with triethylamine (TEA) gave the crude product. HPLC purification, as described above for **5**, afforded pure apo-**6**, which was analyzed by ESI-MS, calcd molecular weight: 958.5; found: 959.5 $[M+H]^+$. A twofold molar excess of ferrous ammonium sulfate ($Fe(NH_4)_2(SO_4)_2$) (aq) was added to give Fe^{II}-loaded **6** immediately preceding affinity cleavage experiments.

NH$_2$-AcrDprLysLys(EDTA·Fe)-CONH$_2$ (7). Rink amide MBHA resin (0.64 mmol g^{-1}, 25 mg, 0.016 mmol) was added to a Bio-Rad Poly-Prep column and swollen in DMF, followed by deprotection of the Fmoc group with 20% piperidine in DMF (3×3 min). After washes of DMF and MeOH, a solution of Fmoc-Lys(Mtt)-OH (5 equiv, Mtt = methyltrityl), HOBt (5 equiv), and HBTU (5 equiv) in DMF was added to the resin, followed immediately by addition of DIPEA (10 equiv). Subsequent Fmoc-protected amino acid couplings of apo-**7** were identical to the preparation of **5**. Before Fmoc deprotection of the acridine residue, the solid support was treated with 1% TFA and 5% TIPS in DCM (2×30 min) to remove the Mtt protecting group of the C-terminal lysine, leaving other acid-labile protecting groups intact.[37] EDTA-monoanhydride was coupled, Fmoc was removed from the acridine residue, and apo-**7** was released from the solid support. Work-up and purification were performed as described previously. ESI-MS, calcd molecular weight: 958.5; found: 959.5 $[M+H]^+$. A twofold molar excess of $Fe(NH_4)_2(SO_4)_2$ (aq) was added to give Fe^{II}-loaded **7** immediately preceding the affinity cleavage experiments.

RNA synthesis and 5′-^{32}P labeling. The 61-nucleotide wild-type RNA was generated by run-off transcription with T7 RNA polymerase. First, an 86-nucleotide dsDNA PCR product was amplified from a chemically synthesized template by using 25-mer and 45-mer DNA oligonucleotide primers. Sequences are as follows: 25-mer, 5′-GAGCGTCAGTCTTCGTCCAGGCCGA-3′; 45-mer, 5′-GCGAATTCTAATACGACTCACTCTCGGGCGGTTTTTCGAAGCTTG-3′, the T7 promoter is underlined; 61-mer template, 5′-GAGCGTCAGTCTTCGTCCAGGCCGAAGCCCTCTACGAGACTCAAGCTTCGAAAAACCGCCC-3′. The PCR product was extracted with phenol/chloroform, precipitated with ethanol, and dissolved in 100 μL reaction volumes consisting of transcription buffer (80 mM HEPES, 25 mM $MgCl_2$, 2 mM spermidine, 30 mM dithiothreitol (DTT), pH 7.5), NTPs (8 mM), and RNase inhibitor (1 U μL^{-1}). Transcription was initiated with T7 RNA polymerase (0.03 mg mL^{-1}) and continued overnight at 40 °C. The reaction mixture was treated with RNase-free DNase I (0.5 U μL^{-1}) and $CaCl_2$ (1 mM) for 1 h at 40 °C and purified on a 10.5% denaturing polyacrylamide gel. The transcribed RNA was visualized by UV shadowing, excised from the gel, and eluted overnight by the crush-and-soak method. After filtration, the solution was extracted with phenol/chloroform and precipitated with ethanol. The RNA concentration was determined by measuring the absorbance at 260 nm. For the preparation of 5′-^{32}P RNA, the transcript (30 pmol) was treated with SAP (0.1 U μL^{-1}) for 45 min at 37 °C, followed by heat inactivation of the enzyme for 15 min at 65 °C. The dephosphorylated RNA was immediately treated with T4 PNK (0.5 U μL^{-1}), [γ-^{32}P]-ATP (2 mCi mL^{-1}) and DTT (1 mM) and incubated for 45 min at 37 °C. Labeled RNA was gel purified, visualized by storage phosphor autoradiography, and isolated as previously described.

The 60-nucleotide mutant RNA construct was chemically synthesized on a Perkin–Elmer/ABI Model 392 DNA/RNA synthesizer with β-cyanoethyl phosphoramidites purchased from Glen Research (Sterling, VA). The 5′-*O*-dimethoxytrityl (DMT) and 2′-*O*-tertbutyldimethylsilyl (TBDMS) phosphoramidites were deprotected with ammonium hydroxide/ethanol, followed by triethylamine-3HF. The oligonucleotides were gel purified and 5′-^{32}P end-labeled, as described above.

Affinity cleaving. HTPs **6** and **7** and MPE·Fe were incubated with 5′-^{32}P-labeled wild-type and mutant RNAs (1 nM) for 15 min in reaction buffer at ambient temperature. The resulting complexes were probed by initiating hydroxyl-radical formation through the addition of hydrogen peroxide (0.01%) and DTT (5 mM). The reactions were allowed to proceed for 20 min at room temperature, then quenched by the addition of distilled, deionized water. This was followed by phenol/chloroform extraction and ethanol precipitation. Cleaved RNA was resuspended in formamide loading buffer, heat denatured, and analyzed by denaturing 10.5% PAGE.

Gel mobility shift assay. To observe the inhibition of the protein–RNA complexes, increasing concentrations of **6** were incubated with *E. coli* S15 (100 nM) and 5′-^{32}P-labeled wild-type and mutant RNAs (100 pM) in reaction buffer at 0 °C for 30 min. The complexes were resolved from free RNA by native 8% polyacrylamide (29:1 acrylamide/bis) gel electrophoresis. Optimal resolution was obtained by running the gel at 4 °C with a 90 V potential for 5.5 h.

Quantitative RNase V1 footprinting. Dissociation constants for **5**, ethidium bromide, and S15 on the wild-type and mutant RNAs

were obtained by using RNase V1 under native conditions. Ligand/protein–RNA complexes were formed by incubating increasing concentrations of the ligand/protein with 5′-^{32}P-labeled RNA (1 nM) for 15 min in reaction buffer (50 mM Bis-Tris·HCl, pH 7.0, 100 mM NaCl, 10 mM $MgCl_2$, and 10 μg mL^{-1} yeast tRNA^{Phe}) at ambient temperature. Enzymatic digestions with RNase V1 (0.0001 U μL^{-1}) were carried out for 30 min at ambient temperature and quenched with hot, formamide loading buffer. Cleaved RNA was heat denatured and analyzed by 10.5% denaturing PAGE. The cleavage efficiency at nucleotide(s) near the binding site was calculated by normalizing for any differential loading of each concentration of the ligand or protein tested.

For HTP **5** and ethidium bromide bound to the wild-type RNA, the footprint at A663 was monitored with respect to the V1-dependent constant band C651. For the same ligands bound to the mutant RNA, the footprint at G661 was monitored with respect to the same constant band. The cleavage data for the RNA were converted to binding data for the ligand by assuming that the maximum cleavage efficiency corresponds to 0% occupancy and the minimum cleavage efficiency corresponds to 100% occupancy. The fraction of RNA bound by the ligand was plotted as a function of concentration, and the data were fitted to the equation: fraction of RNA bound = [ligand]/([ligand]+K_d). Dissociation constants are reported as the average and standard deviation of three different experiments.

For S15 bound to the wild-type RNA, hyperreactivity at A663 was followed with respect to the V1-dependent constant band U590. The cleavage data for the RNA were converted to binding data for the protein by assuming that the minimum cleavage efficiency corresponds to 0% occupancy and the maximum cleavage efficiency corresponds to 100% occupancy. However, for S15 bound to the mutant RNA, the hyperreactive pattern was not observed. Instead, a footprint at C658–U659 was monitored with respect to U594, and cleavage data were processed by assuming that the maximum cleavage efficiency corresponds to 0% occupancy and the minimum cleavage efficiency corresponds to 100% occupancy. The fraction of RNA bound by S15 was plotted as a function of concentration, and the data were fitted to the equation: fraction RNA bound = [S15]/([S15]+K_d). The results are reported as the average and standard deviation of three different experiments (see Supporting Information).

Acknowledgements

P.A.B. acknowledges support from the NIH (AI-49062). We also thank Dr. Robyn Hickerson and Prof. Harry Noller (UCSC) for their generous donation of *E. coli* S15.

Keywords: intercalation · peptides · ribosomes · RNA recognition · RNA

[1] M. J. Drysdale, G. Lentzen, N. Matassova, A. I. Murchie, F. Aboul-ela, M. Afshar, *Prog. Med. Chem.* **2002**, *39*, 73.
[2] J. Gallego, G. Varani, *Acc. Chem. Res.* **2001**, *34*, 836.
[3] K. L. McKnight, B. A. Heinz, *Antiviral Chem. Chemother.* **2003**, *14*, 61.
[4] Y. Tor, *ChemBioChem* **2003**, *4*, 998.
[5] S. H. L. Verhelst, P. J. A. Michiels, G. A. van der Marel, C. A. A. van Boeckel, J. H. van Boom, *ChemBioChem* **2004**, *5*, 937.
[6] M. Froeyen, P. Herdewijn, *Curr. Top. Med. Chem.* **2002**, *2*, 1123.
[7] W. D. Wilson, K. Li, *Curr. Med. Chem.* **2000**, *7*, 73.
[8] C. B. Carlson, P. A. Beal, *Bioorg. Med. Chem. Lett.* **2000**, *10*, 1979.
[9] C. B. Carlson, P. A. Beal, *Org. Lett.* **2000**, *2*, 1465.
[10] C. B. Carlson, R. J. Spanggord, P. A. Beal, *ChemBioChem* **2002**, *3*, 859.
[11] C. B. Carlson, P. A. Beal, *J. Am. Chem. Soc.* **2002**, *124*, 8510.
[12] C. B. Carlson, M. Vuyisich, B. D. Gooch, P. A. Beal, *Chem. Biol.* **2003**, *10*, 663.
[13] B. D. Gooch, P. A. Beal, *J. Am. Chem. Soc.* **2004**, *126*, 10603.
[14] M. Krishnamurthy, B. D. Gooch, P. A. Beal, *Org. Lett.* **2004**, *6*, 63.
[15] A. Malina, S. Khan, C. B. Carlson, Y. Svitkin, I. Harvey, N. Sonenberg, P. A. Beal, J. Pelletier, *FEBS Lett.* **2005**, *579*, 79.
[16] I. Calin-Jageman, A. K. Amarasinghe, A. W. Nicholson, *Nucleic Acids Res.* **2001**, *29*, 1915.
[17] J. M. Kean, S. A. White, D. E. Draper, *Biochemistry* **1985**, *24*, 5062.
[18] N. K. Tanner, T. R. Cech, *Nucleic Acids Res.* **1985**, *13*, 7759.
[19] N. K. Tanner, T. R. Cech, *Nucleic Acids Res.* **1985**, *13*, 7741.
[20] S. A. White, D. E. Draper, *Nucleic Acids Res.* **1987**, *15*, 4049.
[21] S. A. White, D. E. Draper, *Biochemistry* **1989**, *28*, 1892.
[22] S. Nonin, F. Jiang, D. J. Patel, *J. Mol. Biol.* **1997**, *268*, 359.
[23] S. C. Agalarov, G. S. Prasad, P. M. Funke, C. D. Stout, J. R. Williamson, *Science* **2000**, *288*, 107.
[24] A. Nikulin, A. Serganov, E. Ennifar, S. Tishchenko, N. Nevskaya, W. Shepard, C. Portier, M. Garber, B. Ehresmann, C. Ehresmann, S. Nikonov, P. Dumas, *Nat. Struct. Biol.* **2000**, *7*, 273.
[25] W. A. Held, B. Ballou, S. Mizushima, M. Nomura, *J. Biol. Chem.* **1974**, *249*, 3103.
[26] I. Jagannathan, G. M. Culver, *J. Mol. Biol.* **2003**, *330*, 373.
[27] P. Svensson, L. M. Changchien, G. R. Craven, H. F. Noller, *J. Mol. Biol.* **1988**, *200*, 301.
[28] P. B. Dervan, *Science* **1986**, *232*, 464.
[29] H. Han, P. B. Dervan, *Nucleic Acids Res.* **1994**, *22*, 2837.
[30] H. E. Moser, P. B. Dervan, *Science* **1987**, *238*, 645.
[31] W. K. Pogozelski, T. D. Tullius, *Chem. Rev.* **1998**, *98*, 1089.
[32] J. S. Taylor, P. G. Schultz, P. B. Dervan, *Tetrahedron* **1984**, *40*, 457.
[33] A. Serganov, L. Bénard, C. Portier, E. Ennifar, M. Garber, B. Ehresmann, C. Ehresmann, *J. Mol. Biol.* **2001**, *305*, 785.
[34] V. V. Vlassov, G. Zuber, B. Felden, J. P. Behr, R. Giege, *Nucleic Acids Res.* **1995**, *23*, 3161.
[35] D. Klostermeier, P. Sears, C.-H. Wong, D. P. Millar, J. R. Williamson, *Nucleic Acids Res.* **2004**, *32*, 2707.
[36] Y. W. Ebright, Y. P. Chen, S. Pendergrast, R. H. Ebright, *Biochemistry* **1992**, *31*, 10664.
[37] C. Park, K. Burgess, *J. Comb. Chem.* **2001**, *3*, 257.

Received: July 8, 2005
Published online on October 24, 2005

